

Analytical expressions for singular integrals arising from the 3D Laplace and Stokes kernels when using constant or linear triangular and quadrilateral boundary elements

Jure Ravnik

Faculty of Mechanical Engineering, University of Maribor, Smetanova 17, SI 2000, Maribor, Slovenia

ARTICLE INFO

Keywords:

Singular integrals
 Triangular boundary elements
 Quadrilateral boundary elements
 Laplace equation
 Creeping flow
 Stokes problem
 Analytical expression

ABSTRACT

In this paper we present analytical expressions for the computation of singular integrals obtained in the discretisation of boundary integral equations for the Laplace and creeping flow (Stokes) problems with triangular or quadrilateral boundary elements with linear interpolation of the potential and constant interpolation of the flux. We compare the singular integrals computed with the presented analytical expressions with the same integrals computed with numerical quadrature and find that a considerably larger computational effort has to be made for numerical quadrature to achieve high accuracy than with the analytical expression. Furthermore, we show that the accuracy in solving a Laplace test case and a creeping flow test case using analytical expressions for singular integrals is better than the accuracy achieved with numerical quadrature. The analytical expressions are listed in the appendix of the paper and their implementation in computer code is available online.

1. Introduction

It is well known that when applying the Boundary Element Method (BEM) to solve any engineering problem, singular integrals must be evaluated. Since this is a challenge for numerical implementation, many efforts [1–17] have been made to develop methods for efficient and accurate computation of these singular integrals. Various schemes such as the polar coordinate transformation, the singularity subtraction method, polynomial transformation method [18], distance transformation method [19], special quadratures, interval subdivision method [20,21], variable transformation methods, recursive algorithms, etc., have been developed. Researchers [22–25] have also considered nearly singular integrals, which occur when the source point is close but not on the boundary element. Some researchers [26] propose semi-analytical approaches to calculate singular integrals in isogeometric boundary element method for potential problem. To this day, numerical quadrature schemes [27–30] are developed with the aim of calculation of singular integrals arising from boundary integral equations. A wide variety of research topics in sciences and engineering was targeted, for example a numerical integration scheme for Stokes flow was presented by [31].

The singular integrals can be calculated most efficiently if an analytical expression for the solution is found (see [32]). In most cases, using an analytical expression saves computational time and guarantees high accuracy of the resulting integral value. It is almost impossible to find

a general expression for the singular integral because it depends not only on the Green's function that forms the kernel of the integral, but also on the type of boundary element used, the position of the source point within the element, the interpolation scheme used and whether the problem is viewed in 2D or 3D. However, by choosing the Green's function, the interpolation scheme and the type of boundary element, it is possible to find analytical expressions for singular integrals for different source point positions.

Ren and Chan [33] proposed a method for deriving analytical expressions for a singular integrals. They proposed to map a triangular boundary element in 3D space to a reference triangle in a plane where analytical integration is possible. They provided analytical expressions for constant triangular elements for Laplace and Stokes kernels. In this paper we extend their work to linear triangular and quadrilateral elements with linear interpolation of the function and constant interpolation of the flux. We also present an algorithm to construct an analytical expression for each singular boundary element defined in a plane. The presented expressions are new and will be useful to the developers of BEM codes, as they will be able to avoid complicated numerical quadrature algorithms with numerical parameters that lead to unknown accuracy in the computation of singular integrals. To make it easier for other researchers to use the analytical expressions, we have included a computer code implementation of the derived analytical expressions in the supplementary material [34].

E-mail address: jure.ravnik@um.si.

<https://doi.org/10.1016/j.enganabound.2023.02.057>

Received 13 July 2022; Accepted 28 February 2023

0955-7997/© 2023 The Author(s). Published by Elsevier Ltd. This is an open access article under the CC BY-NC-ND license (<http://creativecommons.org/licenses/by-nc-nd/4.0/>).

The paper is structured as follows: In Section 2 we briefly introduce the boundary integral equations for the Laplace and creeping flow problems. In Section 3 we derive the expression for the singular integrals. The expressions themselves are given in the appendix. In Section 4 we compare analytical expressions with numerical quadrature and in Section 5 we present two test cases for the Laplace and Stokes equations using analytical expressions for singular integrals. The last section contains the conclusions.

2. Boundary integral equations

In this section we introduce the boundary integral equations and the associated singular integrals for the Laplace equation and the creeping flow problem (the Stokes equation). We include only an overview of the numerical algorithm, additional details are given in our previous works [35–38], where our BEM solution of these problems is given in all detail.

2.1. The Laplace equation

Let the unknown potential be denoted by u and defined in 3D with a position vector $\vec{r} \in \mathbb{R}^3$. The boundary integral representation of the Laplace equation, $\nabla^2 u = 0$, can be written as [39]:

$$c(\vec{\xi})u(\vec{\xi}) + \int_{\Gamma} u \vec{\nabla} u^* \cdot \vec{n} d\Gamma = \int_{\Gamma} u^* \underbrace{(\vec{n} \cdot \vec{\nabla} u)}_q d\Gamma, \quad \vec{\xi} \in \Gamma, \quad (1)$$

where Γ is the domain boundary, $\vec{\xi}$ is the source point at the boundary, \vec{n} is the normal on the boundary and c is the free coefficient. Defining $\hat{r} = \vec{r} - \vec{\xi}$ and $r = |\hat{r}|$ we can write the fundamental solution of the Laplace operator and its gradient as $u^* = -1/(4\pi r)$ and $\vec{\nabla} u^* = -\hat{r}/(4\pi r^3)$, respectively. Such a representation enables us to only solve for the unknowns at the boundary of the domain, since the solution in the interior depends only of the knowledge of boundary variables (potential u and flux $q = \vec{n} \cdot \vec{\nabla} u$).

To obtain a system of linear equations for the unknowns at the boundary, we discretise the boundary with boundary elements. Within boundary elements we use linear interpolation of potential $u = \sum \Phi_i u_i$ and constant interpolation of flux. Using this interpolation scheme one must calculate the following integrals on each boundary element l :

$$H_i^{(l)} = \int_{\Gamma_l} \Phi_i \vec{\nabla} u^* \cdot \vec{n} d\Gamma, \quad G^{(l)} = \int_{\Gamma_l} u^* d\Gamma. \quad (2)$$

By placing the source points in all (potential and flux) boundary nodes, and taking note of the boundary conditions, we are able to set up a system of linear equations, which can be solved for the unknown boundary variables. This approach has been used by Šušnjara et al. [35,36] using purely numerical integration routines to solve an electrostatics problem.

2.2. The Stokes equation

We consider the steady incompressible flow of a Newtonian fluid at very small Reynolds numbers, i.e. $Re \ll 1$, where we can neglect the advection term in the Navier–Stokes equations, leading to the equations of creeping flow (Stokes):

$$\vec{\nabla} \cdot \vec{u} = 0, \quad \vec{\nabla} \cdot \underline{\sigma} + \rho \vec{g} = 0. \quad (3)$$

Here \vec{u} is the flow velocity, ρ is the fluid density and \vec{g} is the gravitational acceleration. The Cauchy stress tensor $\underline{\sigma}$ is defined as $\underline{\sigma} = -P\underline{I} + \underline{\tau}$, where P is the pressure, \underline{I} the identity tensor, and $\underline{\tau}$ the viscous stress tensor. A Newtonian model for the viscous stress tensor $\tau_{ij} = \mu \left[\frac{\partial u_i}{\partial x_j} + \frac{\partial u_j}{\partial x_i} \right]$ leads to the following form of the Stokes equation

$$-\vec{\nabla} P + \mu \nabla^2 \vec{u} + \rho \vec{g} = 0, \quad (4)$$

where μ is the fluid viscosity. Finally, we recognise, that gravity is a conservative force, which may be written as a gradient of the gravitational potential and introduce a modified pressure as $p = P - \rho\Phi$, where $\vec{g} = \vec{\nabla}\Phi$. With this, the final form of the Stokes equation is:

$$-\vec{\nabla} p + \mu \nabla^2 \vec{u} = 0. \quad (5)$$

The Stokes flow Green’s functions satisfy the continuity equation $\vec{\nabla} \cdot \vec{u} = 0$ and are the solutions of the singularly forced Stokes equation. The 3D free-space Green’s functions are

$$G_{ij}^* = \frac{\delta_{ij}}{r} + \frac{\hat{r}_i \hat{r}_j}{r^3}, \quad T_{ijk}^* = -6 \frac{\hat{r}_i \hat{r}_j \hat{r}_k}{r^5}. \quad (6)$$

The boundary integral representation for the Stokes problem is [40]:

$$c(\vec{\xi})u_j(\vec{\xi}) = \int_{\Gamma}^{PV} u_i T_{ijk}^* n_k d\Gamma - \frac{1}{\mu} \int_{\Gamma} G_{ji}^* q_i d\Gamma, \quad (7)$$

where $c(\vec{\xi}) = 2\alpha$ is twice the solid angle as seen from the point $\vec{\xi}$, i.e. in the interior of the domain $c = 8\pi$, at a smooth boundary $c = 4\pi$. The normal vector \vec{n} points into the domain. The terms on the right represent the double and single layer potentials of the three-dimensional Stokes flow. To derive a discrete version of (7) we consider the boundary $\Gamma = \sum_l \Gamma_l$ to be decomposed into boundary elements Γ_l :

$$c(\vec{\xi})u_j(\vec{\xi}) = \sum_l \int_{\Gamma_l}^{PV} u_i T_{ijk}^* n_k^{(l)} d\Gamma - \frac{1}{\mu} \sum_l \int_{\Gamma_l} G_{ji}^* q_i d\Gamma, \quad (8)$$

where $n_k^{(l)}$ is the k component of the normal vector pointing from boundary element l into the domain.

Let Φ be the interpolation functions used to interpolate the function values within boundary elements, i.e. $u_i = \sum_m \Phi_m u_i^{(l,m)}$, where $u_i^{(l,m)}$ is the m th nodal value of function within l th boundary element. Constant interpolation is considered for flux. This yields:

$$c(\vec{\xi})u_j(\vec{\xi}) = \sum_l \sum_m u_i^{(l,m)} \int_{\Gamma_l}^{PV} \Phi_m T_{ijk}^* n_k^{(l)} d\Gamma - \frac{1}{\mu} \sum_l q_i^{(l)} \int_{\Gamma_l} G_{ji}^* d\Gamma. \quad (9)$$

The following integrals must be calculated for each boundary element l :

$$T_{ij}^{(l,m)}(\vec{\xi}) = \int_{\Gamma_l}^{PV} \Phi_m T_{ijk}^* n_k^{(l)} d\Gamma, \quad G_{ij}^{(l)}(\vec{\xi}) = \int_{\Gamma_l} G_{ij}^* d\Gamma. \quad (10)$$

Considering boundary conditions we can place the source point into nodes, where unknown values are located and produce a system of linear equations for the velocity and traction. This approach has been used by Štrákl et al. [37,38] to estimate the force acting on a particle in Stokes flow, where additional details can be found. Their implementation used solely numerical integration.

3. Evaluation of singular integrals

3.1. Triangular elements

To derive the analytical expressions for singular integrals we first translate, rotate and map the boundary element onto a reference triangle on a plane. This converts a surface integral in 3D space to a double integral over a reference triangle. The procedure was proposed Ren and Chan [33] and is sketched in Fig. 1. The boundary element is initially defined in the frame of reference O_1 with nodes \vec{a}_1 , \vec{b}_1 and \vec{c}_1 . Its barycentre is at $\vec{s}_1 = (\vec{a}_1 + \vec{b}_1 + \vec{c}_1)/3$. We use translation to set the origin of the frame of reference O_2 into the barycentre of the element with $\vec{a}_2 = \vec{a}_1 - \vec{s}_1$, $\vec{b}_2 = \vec{b}_1 - \vec{s}_1$ and $\vec{c}_2 = \vec{c}_1 - \vec{s}_1$. Next, we define an orthonormal basis $(\vec{x}_r, \vec{y}_r, \vec{z}_r)$ with origin at O_2 and \vec{z}_r pointing in the normal direction by

$$\vec{x}_r = \frac{\vec{b}_2 - \vec{a}_2}{|\vec{b}_2 - \vec{a}_2|}, \quad \vec{z}_r = \frac{(\vec{c}_2 - \vec{a}_2) \times \vec{x}_r}{|(\vec{c}_2 - \vec{a}_2) \times \vec{x}_r|}, \quad \vec{y}_r = \frac{\vec{z}_r \times \vec{x}_r}{|\vec{z}_r \times \vec{x}_r|}. \quad (11)$$

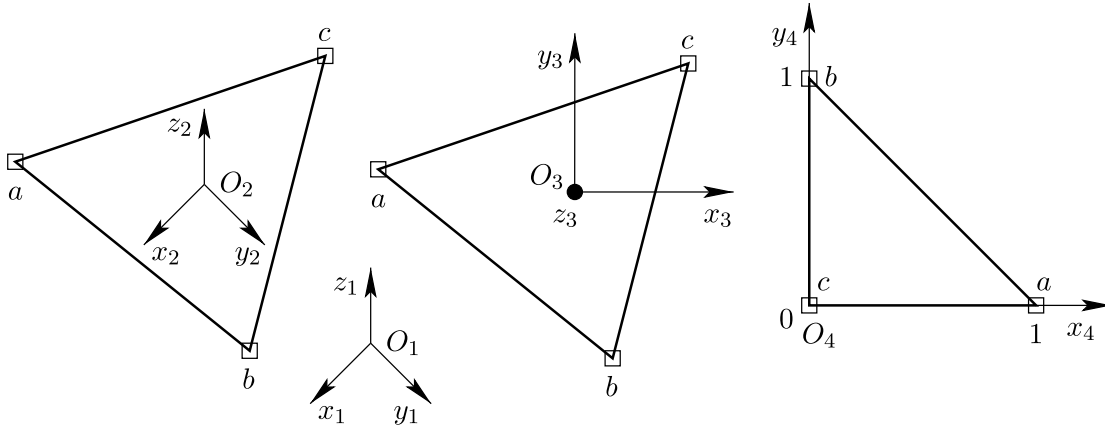


Fig. 1. Translation ($O_1 \rightarrow O_2$), rotation ($O_2 \rightarrow O_3$) and mapping ($O_3 \rightarrow O_4$) of a triangular boundary element to a reference triangle on the (x_4, y_4) plane.

Defining the bases $\hat{i} = (1, 0, 0)$, $\hat{j} = (0, 1, 0)$ and $\hat{k} = (0, 0, 1)$ we define a rotation matrix for the ($O_2 \rightarrow O_3$) rotation as

$$\underline{R} = \begin{pmatrix} \bar{x}_r \cdot \hat{i} & \bar{x}_r \cdot \hat{j} & \bar{x}_r \cdot \hat{k} \\ \bar{y}_r \cdot \hat{i} & \bar{y}_r \cdot \hat{j} & \bar{y}_r \cdot \hat{k} \\ \bar{z}_r \cdot \hat{i} & \bar{z}_r \cdot \hat{j} & \bar{z}_r \cdot \hat{k} \end{pmatrix}. \quad (12)$$

Now, we can calculate the element node locations in O_3 as $\bar{a}_3 = \underline{R} \cdot \bar{a}_2$, $\bar{b}_3 = \underline{R} \cdot \bar{b}_2$ and $\bar{c}_3 = \underline{R} \cdot \bar{c}_2$. Since the z_3 axis is normal to the plane in which the element is located, the z components of \bar{a}_3 , \bar{b}_3 and \bar{c}_3 are zero.

Next we map \bar{a}_3 to $(1,0)$, \bar{b}_3 to $(0,1)$ and \bar{c}_3 to $(0,0)$ in O_4 frame of reference (here we omit z components as they are all zero). Setting the origin for frame of reference O_4 to node c , we derive the mapping matrix by requiring

$$\underline{M} \cdot \begin{pmatrix} 1 \\ 0 \end{pmatrix} = \begin{pmatrix} a_{3,x} - c_{3,x} \\ a_{3,y} - c_{3,y} \end{pmatrix}, \quad \underline{M} \cdot \begin{pmatrix} 0 \\ 1 \end{pmatrix} = \begin{pmatrix} b_{3,x} - c_{3,x} \\ b_{3,y} - c_{3,y} \end{pmatrix}, \quad (13)$$

which yields the mapping matrix

$$\underline{M} = \begin{pmatrix} m_{11} & m_{12} \\ m_{21} & m_{22} \end{pmatrix} = \begin{pmatrix} a_{3,x} - c_{3,x} & b_{3,x} - c_{3,x} \\ a_{3,y} - c_{3,y} & b_{3,y} - c_{3,y} \end{pmatrix}. \quad (14)$$

3.1.1. The Laplace kernel

Let us consider a single triangular boundary element Γ_l and consider how to express the integrals (2). The source point $\bar{\xi} = (\xi, \eta, \zeta)$ is located at one of the nodes of the element (for linear interpolation scheme used for function) or in the barycentre of the element (for constant interpolation scheme used for flux). As the source point is located on the element, the term $(\bar{r} - \bar{\xi}) \cdot \bar{n}$ is identically equal to zero for all \bar{r} in the element. Thus, all H integrals are zero. We write the G integrals in frame of reference O_3 as:

$$G^{Laplace} = -\frac{1}{4\pi} \int_{\Gamma_l} \frac{d\Gamma_3}{\sqrt{(x_3 - \xi_3)^2 + (y_3 - \eta_3)^2}} \quad (15)$$

Since the boundary element in frame of reference O_3 lies in the (x_3, y_3) plane, the term $z_3 - \zeta_3$ is zero everywhere, so it was omitted from Eq. (15).

Frame of reference O_4 is a reference triangle with vertexes in $(1,0,0)$, $(0,1,0)$ and $(0,0,0)$. The source points we consider are located at the vertexes and at the barycentre of the element, i.e. $\bar{\xi}_4 = (1, 0, 0)$, $\bar{\xi}_4 = (0, 1, 0)$, $\bar{\xi}_4 = (0, 0, 0)$ and $\bar{\xi}_4 = (1/3, 1/3, 0)$. We use the mapping (14) to connect O_4 with O_3 as:

$$\begin{pmatrix} x_3 - \xi_3 \\ y_3 - \eta_3 \end{pmatrix} = \begin{pmatrix} m_{11} & m_{12} \\ m_{21} & m_{22} \end{pmatrix} \cdot \begin{pmatrix} x_4 - \xi_4 \\ y_4 - \eta_4 \end{pmatrix} \quad (16)$$

When inserting (16) into (15) one obtains the following expression or the integral in frame of reference O_4 :

$$G^{Laplace} = -\frac{J}{4\pi} \int_0^1 \int_0^{1-x} \frac{dy dx}{\sqrt{a(x - \xi_4)^2 + b(y - \eta_4)^2 + c(x - \xi_4)(y - \eta_4)}} \quad (17)$$

with Jacobian $J = 2A$, where A is the area of the original triangle, and $a = m_{11}^2 + m_{21}^2$, $b = m_{12}^2 + m_{22}^2$, $c = 2(m_{11}m_{12} + m_{21}m_{22})$. The integral can be analytically solved for all considered locations of the source point. The results is:

$$G^{Laplace} = -\frac{J}{4\pi} \mathcal{F}, \quad (18)$$

where the \mathcal{F} value depends on the placement of the source point. Analytical expressions for \mathcal{F} with source points placed in $\bar{\xi}_4 = (1, 0, 0)$, $\bar{\xi}_4 = (0, 1, 0)$, $\bar{\xi}_4 = (0, 0, 0)$ and $\bar{\xi}_4 = (1/3, 1/3, 0)$ are given in Appendix.

3.1.2. The Stokes kernels

When considering the singular integrals with the Stokes kernel (10) we again translate ($O_1 \rightarrow O_2$), rotate ($O_2 \rightarrow O_3$) and map ($O_3 \rightarrow O_4$) the triangular boundary element to a reference triangle in the (x_4, y_4) plane (see Fig. 1). As the source point is in the same plane as the element, the dot product of a vector in the plane of the boundary element with the boundary element normal is zero, so $T_{ij} = 0$. Looking at the kernel of the G_{ij} integrals (6), we notice that due to symmetry we have $G_{ij} = G_{ji}$ and that the $1/r$ term, which is present only for G_{ii} , is the same as the Laplace kernel. This means that for the $1/r$ term we can use the already derived expressions for \mathcal{F} , and focus here solely on the $1/r^3$ term.

For example, for $i = x, j = y$, the integral of the $1/r^3$ term in frame of reference O_3 can be expressed as:

$$G'_{xy} = \int_{\Gamma} \frac{(x_3 - \xi_3)(y_3 - \eta_3)}{((x_3 - \xi_3)^2 + (y_3 - \eta_3)^2)^{3/2}} d\Gamma_3 \quad (19)$$

Making use of (14) and considering the source point to be at (ξ_4, η_4) within the reference triangle, Eq. (19) can be expressed in the reference triangle for the general G'_{ij} case as

$$G'_{ij} = J \int_0^1 \int_0^{1-x} \frac{d_{ij}(x - \xi_4)^2 + e_{ij}(y - \eta_4)^2 + f_{ij}(x - \xi_4)(y - \eta_4)}{(a(x - \xi_4)^2 + b(y - \eta_4)^2 + c(x - \xi_4)(y - \eta_4))^{3/2}} dy dx \quad (20)$$

with Jacobian $J = 2A$, where A is the area of the original triangle, $a = m_{11}^2 + m_{21}^2$, $b = m_{12}^2 + m_{22}^2$, $c = 2(m_{11}m_{12} + m_{21}m_{22})$ and

$$d_{xx} = m_{11}^2, \quad e_{xx} = m_{12}^2, \quad f_{xx} = 2m_{11}m_{12},$$

$$d_{yy} = m_{21}^2, \quad e_{yy} = m_{22}^2, \quad f_{yy} = 2m_{21}m_{22},$$

$$d_{xy} = m_{11}m_{21}, \quad e_{xy} = m_{12}m_{22}, \quad f_{xy} = m_{11}m_{22} + m_{21}m_{12}.$$

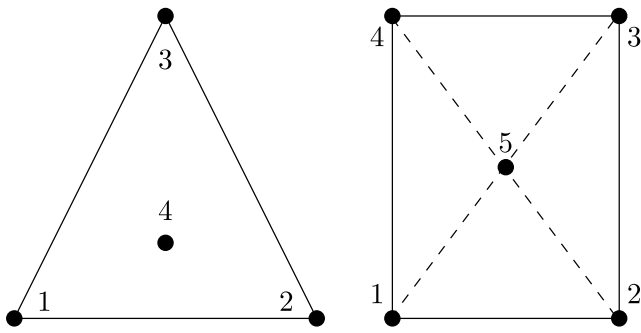


Fig. 2. A triangle and quadrilateral shown on the (x_3, y_3) plane. Source point locations are marked. Dashed lines indicate auxiliary triangles, which are constructed for integration over quadrilaterals.

We note that $d_{xz} = d_{yz} = e_{xz} = e_{yz} = f_{xz} = f_{yz} = 0$ since the reference triangle lies in the (x_4, y_4) plane so the terms involving the z component are zero. After integration, we must rotate the obtained values back to the original frame of reference, since the unknown velocity and traction fields are calculated there. We employ the rotation matrix (12) to do that. The final expression for the integrals in (10) is:

$$G^{Stokes} = J \underline{R}^T \begin{pmatrix} \mathcal{F} + \mathcal{G}_{xx} & \mathcal{G}_{xy} & 0 \\ \mathcal{G}_{xy} & \mathcal{F} + \mathcal{G}_{yy} & 0 \\ 0 & 0 & \mathcal{F} \end{pmatrix} \underline{R} \quad (21)$$

with analytical expressions for \mathcal{F} , \mathcal{G}_{xx} , \mathcal{G}_{xy} , \mathcal{G}_{yy} given in Appendix.

3.2. Quadrilateral elements

We calculate singular integrals on a quadrilateral boundary element by dividing the quadrilateral element into two (or four) triangles and then adding up the analytical expressions for triangular boundary elements. For example, if the source point is in node 1 (see Fig. 2), two triangles are formed with nodes 1-2-3 and 1-3-4 for which formula (18) or (21) can be applied. Similarly, for the source point in node 2, we use two triangles defined by nodes 2-3-4 and 2-4-1. For the source point in node 3, we use nodes 3-4-1 and 3-1-2, and for node 4, we use nodes 4-1-2 and 4-2-3. In the case where the source point is at the centre of the element in node 5, we add values from four triangles consisting of the following node combinations: 5-1-2, 5-2-3, 5-3-4 and 5-4-1.

3.3. Other types of boundary elements

In recent years, many researchers have moved to using meshes with hexagonal or polygonal elements [41]. Regardless of the shape used, each shape can easily be divided into triangles and then the formula (18) or (21) can be used to evaluate each triangle separately, following the same principle we proposed for quadrilateral elements. This gives us the possibility to evaluate singular integrals for virtually any element type, provided that all nodes of the element lie in the same plane.

4. Comparison with numerical integration

In order to test the accuracy of the implemented analytical solutions, we compare them with numerical approaches as described for triangular elements by Šušnjara et al. [35] and for quadrilateral elements proposed by Huang and Cruse [13]. The scheme for triangles uses a recursive subdivision of the domain. Integrals on quadrilaterals are evaluated using the polar coordinate transformation, converting the surface integral into a double integral in the radial and angular directions.

To facilitate comparison of results, we introduce the RMS difference

$$RMS = \left(\frac{\sum_i (a_i - n_i)^2}{\sum_i a_i^2} \right)^{1/2} \quad (22)$$

measuring the difference between results obtained using analytical expression for singular integrals proposed in this paper a_i and the numerical quadrature based results n_i . We measure the RMS difference between the singular integral values calculated analytically and numerically on a selection of test triangular and quadrilateral boundary elements for both the Laplace and the Stokes kernels. We find (Fig. 3) that the numerical values converge towards the analytical results when sufficient computational effort is applied. This is reflected in the CPU time needed for the evaluation, which we also measured. The CPU time ratio between the numerical and analytical evaluation grows exponentially as the numerical evaluation error decreases. We find that the numerical evaluation requires at least 10 times more computing time to achieve an accuracy of 10^{-10} .

So if we use analytical expressions for singular integrals, we save computation time. This is not very important because the number of singular integrals is small compared to the number of all integrals to be calculated. However, it should be noted that when integrating singular integrals numerically, the computational effort has to be adapted specifically for singular integrals and is not the same as for regular integrals. Moreover, it is difficult to estimate the error involved in the numerical integration of singular integrals or their rate of convergence [29], even when working with a regularisation approach. When an analytical expression is used for a singular integral, we not only speed up the algorithm, but more importantly avoid a potential source of error.

5. Test cases

5.1. The Laplace problem

To assess the importance of calculating singular integrals accurately, we solve the Laplace equation in a cylinder. The cylinder consists of three sections of equal length. In each section the diffusivity is constant but different from the other two sections. The cylinder is isolated so that no flux $q = 0$ is prescribed at the wall. There is a constant potential u at the ends of the cylinder. Choosing the cylinder to be 3 units long, the potential at one end $u_0 = 1$ and at the other end $u_3 = 4$, the diffusivities of $\sigma_1 = 2$, $\sigma_2 = 3$ and $\sigma_3 = 4$, one can solve the problem analytically to derive that the flux along the cylinder is $q = 36/13$ and the potential at the interface between the first and second sections is $u_1 = 66/39$ and between the second and third sections is $u_2 = 34/13$. The numerical solution is obtained using a mesh with 13,034 triangular boundary elements. Fig. 4 shows the sketch of the problem and the RMS difference between the BEM solution with and without analytical evaluation of the singular integrals. We can see that if the numerical integration is accurate enough, the results are indistinguishable from the analytical integration results. This was to be expected, since in Fig. 3 shows that near machine accuracy can be achieved in the numerical evaluation of singular integrals as long as sufficient computational resources are available for these evaluations. However, if the numerical integration of singular integrals is not accurate enough (Fig. 4, less than 10 recursive steps), this has a clear impact on the accuracy of the entire numerical procedure.

5.2. The Stokes problem

We consider a spherical particle in an incompressible fluid. A plug flow is assumed, i.e. far away from the particle the fluid flows in a single direction with uniform velocity. The flow velocity is small, as is the particle diameter, so that the Reynolds number is $Re \ll 1$ and the advective transport of momentum can be neglected. Thus, the Navier–Stokes equations simplify to Stokes equations and can be solved

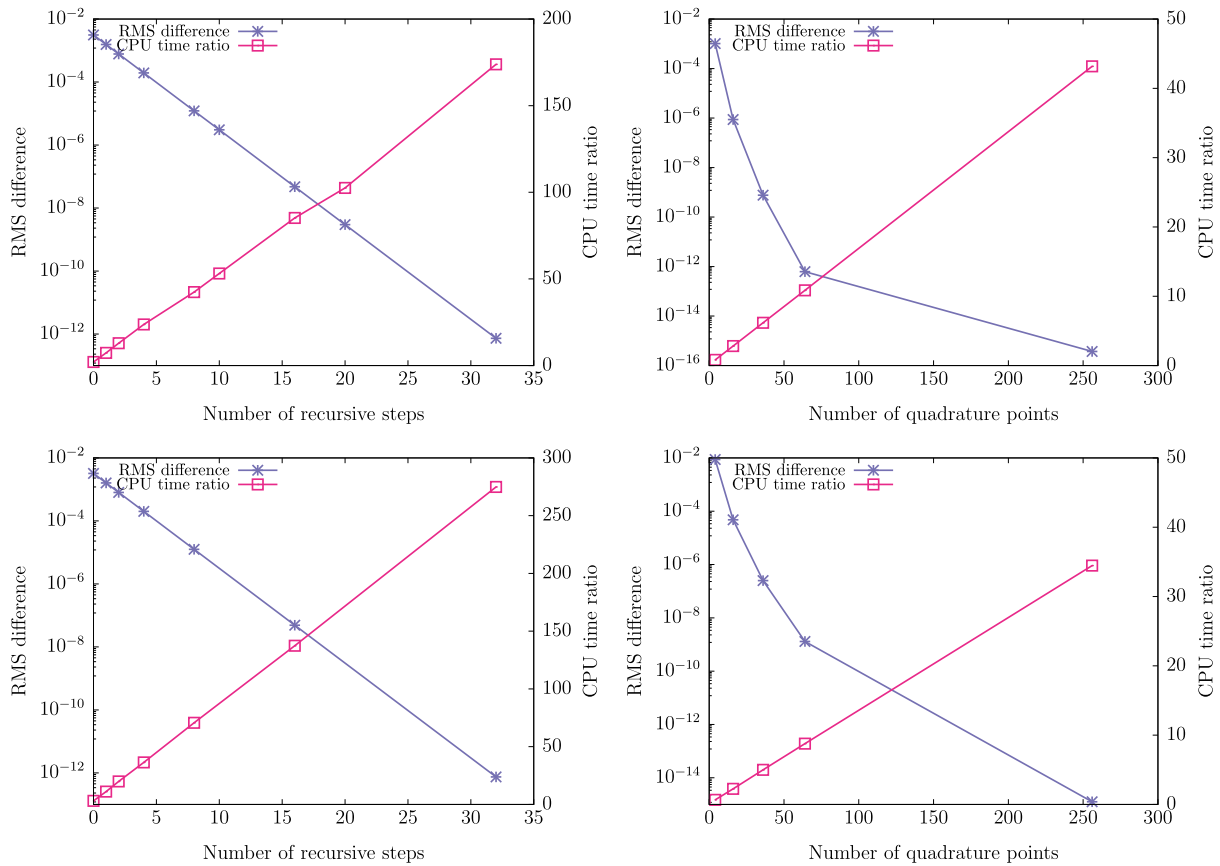


Fig. 3. The RMS difference between the singular integral values calculated by numerical and analytical integration for a triangular (left) and quadrilateral (right) element for the Laplace kernel (top row) and the Stokes kernel (bottom row). Increasing the number of recursive subdivisions of a triangular element in the direction of the singular point in the numerical integration scheme significantly improves the accuracy of the numerical evaluation of the singular integrals, but at the same time the CPU time is significantly longer. Increasing the number of quadrature points for quadrilaterals has the same effect.

analytically [42] for the case of a sphere in plug flow. The resulting force acting on a stationary particle is $F = 3\pi R\mu u_0$, where R is the radius of the particle, μ is the fluid viscosity and u_0 is the plug flow velocity.

We used BEM with analytical and numerical singular integrations to simulate this problem and compare the obtained force on the particle. The sketch of the test case is shown in Fig. 5. The geometry consists of two concentric spheres with a diameter ratio of 1024, where the inner sphere represents the particle. A velocity boundary condition is prescribed for both spheres, namely the plug flow velocity at the outer sphere and the no-slip velocity at the inner sphere (particle). Both spheres are discretised by a total of 5936 triangular boundary elements. The solution gives the flux at the inner sphere which, when integrated over the surface, produces the force. In Fig. 5 we compare the analytical force value and the value obtained by BEM using the analytical or numerical evaluation of the singular integrals. We find that with sufficient computational resources for numerical evaluation of singular integrals, the results are indistinguishable from the case where analytical expressions are used for singular integrals.

6. Conclusions

We presented analytical formulae for calculation of singular integrals when implementing the collocation BEM solution of Laplace or creeping flow (Stokes) problems. Triangular or quadrilateral elements with linear interpolation of function and constant interpolation of flux are considered. The formulae are presented in the Appendix and are implemented into computer code [34] and are freely distributed. We have compared the singular integral values obtained with the presented

formulae with results obtained via numerical quadrature and confirmed that the analytical expressions presented here are indeed correct and that significant reduction of computational time is achieved when using analytical formulae instead of numerical quadrature. We recommend using analytical formulae whenever possible as not only computational time is saved, but more importantly, a source of numerical error is eliminated from the algorithm.

Declaration of competing interest

The authors declare that they have no known competing financial interests or personal relationships that could have appeared to influence the work reported in this paper.

Data availability

Data will be made available on request.

Acknowledgements

The author wishes to thank the Slovenian Research Agency (ARRS) for the financial support in the framework of the Programme P2-0196: Research in Power, Process and Environmental Engineering.

Appendix

We consider source points places into $\vec{\xi}_4 = (1, 0, 0)$, $\vec{\xi}_4 = (0, 1, 0)$, $\vec{\xi}_4 = (0, 0, 0)$ and $\vec{\xi}_4 = (1/3, 1/3, 0)$ and present analytical expression for the singular integrals. Please note that expressions for $\mathcal{F}^{(1/3, 1/3, 0)}$ and

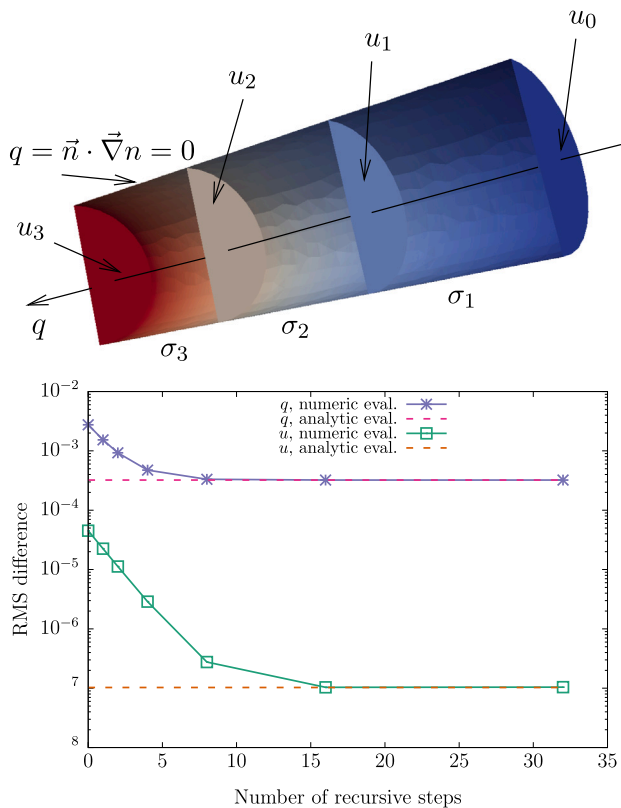


Fig. 4. Top: Sketch for the Laplace problem. Bottom: RMS difference between the analytical solution and the BEM solution for the Laplace problem. The results obtained with purely numerical integration are compared with the results obtained when using the analytical evaluation of singular integrals depending on the number of recursive steps in the numerical integration procedure.

$\mathcal{G}^{1/3,1/3,0}$ have been derived by Ren and Chan [33] (eqs. (24) and (34) in their paper) and are not repeated here.

A computer code implementation of these formulas as well as the associated manipulations of frames of reference, is available at [34].

$$\mathcal{F}^{(0,0,0)} = \frac{\log(2\sqrt{a}\sqrt{a+b-c} + 2a - c) - \log(2\sqrt{b}\sqrt{a+b-c} - 2b + c)}{\sqrt{a+b-c}} \quad (23)$$

$$\mathcal{F}^{(1,0,0)} = \frac{\log(2\sqrt{b}\sqrt{a+b-c} + 2b - c) - \log(2\sqrt{a}\sqrt{b} - c)}{\sqrt{b}} \quad (24)$$

$$\mathcal{F}^{(0,1,0)} = \frac{\log(2\sqrt{a}\sqrt{a+b-c} + 2a - c) - \log(2\sqrt{a}\sqrt{b} - c)}{\sqrt{a}} \quad (25)$$

$$\begin{aligned} \mathcal{G}^{(0,0,0)} = & \frac{1}{b^{3/2}(4ab - c^2)} \left(\frac{b^{3/2}(4ab - c^2)(d + e - f) \log(2\sqrt{a}\sqrt{a+b-c} + 2a - c)}{(a + b - c)^{3/2}} - \right. \\ & \frac{b^{3/2}(4ab - c^2)(d + e - f) \log(2\sqrt{b}\sqrt{a+b-c} - 2b + c)}{(a + b - c)^{3/2}} + \\ & \frac{4ab^{3/2}f + \sqrt{ae}(c^2 - 4ab) \left(\log(2\sqrt{a}\sqrt{b} + c) - 1 \right) - 2a\sqrt{bce} - 2b^{3/2}cd}{\sqrt{a}} + \\ & \frac{2b(-b(2a(e - f) + c(d + f)) + ce(c - a) + 2b^2d)}{a + b - c} + \\ & \left. \frac{2\sqrt{a}\sqrt{b}(b(2a(e - f) + c(d + f)) + ce(a - c) - 2b^2d)}{a + b - c} \right) \end{aligned}$$

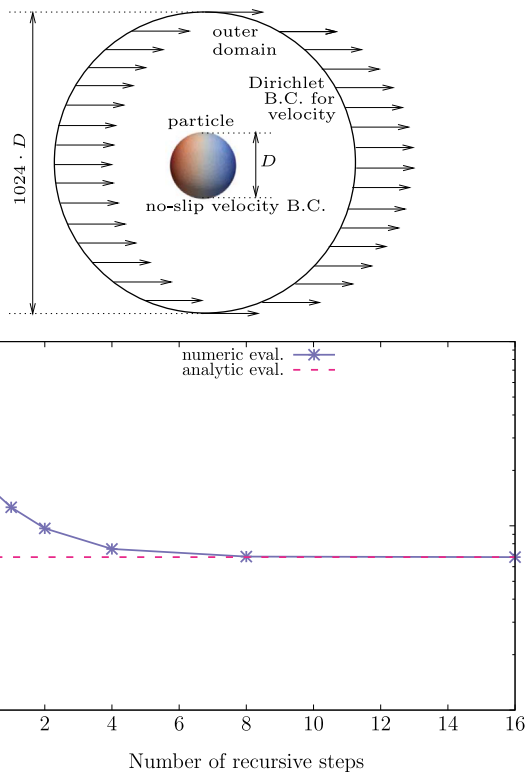


Fig. 5. Top: Sketch for the Stokes problem. Bottom: RMS difference between analytical solution and BEM solution for the force acting on a particle in plug flow under creeping flow conditions. The results obtained with pure numerical integration are compared with the results obtained when using the analytical evaluation of singular integrals depending on the number of recursive steps in the numerical integration procedure.

$$c^2e \log(2\sqrt{a}\sqrt{b} + c) + 4abe \log(2\sqrt{a}\sqrt{b} + c) - 4abe + c^2e \quad (26)$$

$$\begin{aligned} \mathcal{G}^{(1,0,0)} = & \frac{1}{\sqrt{ab}^{3/2}\sqrt{a+b-c}(4ab - c^2)} \left(\right. \\ & 2\sqrt{b} \left(a^{3/2}(-2b(e - f) + ce) + \sqrt{a}(2b^2d - bc(d + f) + c^2e) + \right. \\ & \left. bcd\sqrt{a+b-c} + a\sqrt{a+b-c}(ce - 2bf) \right) - \\ & \left. \sqrt{ae}\sqrt{a+b-c}(4ab - c^2) \cdot \left(\log(2\sqrt{a}\sqrt{b} - c) - \log(2\sqrt{b}\sqrt{a+b-c} + 2b - c) \right) \right) \quad (27) \end{aligned}$$

$$\begin{aligned} \mathcal{G}^{(0,1,0)} = & \frac{1}{b^{3/2}(4ab - c^2)} \left(\frac{1}{a^{3/2}\sqrt{a+b-c}} \left(\right. \right. \\ & \sqrt{a} \left(a^2(4be\sqrt{a+b-c} + 4b^{3/2}f - 2\sqrt{bce}) + \right. \\ & \left. 2b^{3/2}cd(\sqrt{b}\sqrt{a+b-c} - b + c) + \right. \\ & \left. a(-4b^2f\sqrt{a+b-c} - c^2e\sqrt{a+b-c} + 2bce\sqrt{a+b-c} - \right. \\ & \left. 2b^{3/2}c(d + e + 2f) + 4b^{5/2}f + 2\sqrt{bce}e) + \right. \\ & \left. ae\sqrt{a+b-c}(c^2 - 4ab) \log(2\sqrt{b}\sqrt{a+b-c} - 2b + c) \right) + \\ & \left. b^{3/2}d\sqrt{a+b-c}(c^2 - 4ab) \log(2\sqrt{a}\sqrt{b} - c) + \right. \\ & \left. b^{3/2}d\sqrt{a+b-c}(4ab - c^2) \log(2\sqrt{a}\sqrt{a+b-c} + 2a - c) \right) + \\ & \left. \frac{1}{\sqrt{a+b-c}} \left(2\sqrt{b}(b(2a(e - f) + c(d + f)) + ce(a - c) - 2b^2d) + \right. \right. \\ & \left. \left. e\sqrt{a+b-c}(4ab - c^2) \left(\log(2\sqrt{b}\sqrt{a+b-c} - 2b + c) - 1 \right) \right) \right) \quad (28) \end{aligned}$$

References

- [1] Medina DE, Liggett JA. Exact integrals for three-dimensional boundary element potential problems. *Commun Appl Numer Methods* 1989;5(8):555–61. <http://dx.doi.org/10.1002/cnm.1630050809>, <https://onlinelibrary.wiley.com/doi/10.1002/cnm.1630050809>.
- [2] Graglia RD, Lombardi G. Machine precision evaluation of singular and nearly singular potential integrals by use of Gauss quadrature formulas for rational functions. *IEEE Trans Antennas and Propagation* 2008;56(4):981–98. <http://dx.doi.org/10.1109/TAP.2008.919181>, <http://ieeexplore.ieee.org/document/4483591>.
- [3] Carley M. Numerical quadratures for singular and hypersingular integrals in boundary element methods. *SIAM J Sci Comput* 2007;29(3):1207–16. <http://dx.doi.org/10.1137/060666093>, <http://epubs.siam.org/doi/10.1137/060666093>.
- [4] Bremer J, Gimbutas Z. A nystrom method for weakly singular integral operators on surfaces. *J Comput Phys* 2012;231(14):4885–903. <http://dx.doi.org/10.1016/j.jcp.2012.04.003>.
- [5] Kolm P, Rokhlin V. Numerical quadratures for singular and hypersingular integrations. *Comput Math Appl* 2001;41(3–4):327–52. [http://dx.doi.org/10.1016/S0898-1221\(00\)00277-7](http://dx.doi.org/10.1016/S0898-1221(00)00277-7).
- [6] Guiggiani M, Krishnasamy G, Rudolphi TJ, Rizzo FJ. A general algorithm for the numerical solution of hypersingular boundary integral equations. *J Appl Mech* 1992;59(3):604–14. <http://dx.doi.org/10.1115/1.2893766>, <https://asmedigitalcollection.asme.org/appliedmechanics/article/59/3/604/390703/A-General-Algorithm-for-the-Numerical-Solution-of>.
- [7] Khayat M, Wilton D, Fink P. An improved transformation and optimized sampling scheme for the numerical evaluation of singular and near-singular potentials. *IEEE Antennas Wirel Propag Lett* 2008;7:377–80. <http://dx.doi.org/10.1109/LAWP.2008.928461>, <http://ieeexplore.ieee.org/document/4563287>.
- [8] Johnston BM, Johnston PR. A comparison of transformation methods for evaluating two-dimensional weakly singular integrals. *Internat J Numer Methods Engrg* 2003;56(4):589–607. <http://dx.doi.org/10.1002/nme.589>, <https://onlinelibrary.wiley.com/doi/10.1002/nme.589>.
- [9] Gao XW. An effective method for numerical evaluation of general 2D and 3D high order singular boundary integrals. *Comput Methods Appl Mech Engrg* 2010;199(45–48):2856–64. <http://dx.doi.org/10.1016/j.cma.2010.05.008>.
- [10] Wu H, Liu Y, Jiang W. A low-frequency fast multipole boundary element method based on analytical integration of the hypersingular integral for 3D acoustic problems. *Eng Anal Bound Elem* 2013;37(2):309–18. <http://dx.doi.org/10.1016/j.enganabound.2012.09.011>.
- [11] Järvenpää S, Taskinen M, Ylä-Oijala P. Singularity extraction technique for integral equation methods with higher order basis functions on plane triangles and tetrahedra. *Internat J Numer Methods Engrg* 2003;58(8):1149–65. <http://dx.doi.org/10.1002/nme.810>, <https://onlinelibrary.wiley.com/doi/10.1002/nme.810>.
- [12] Nintcheu Fata S. Explicit expressions for 3D boundary integrals in potential theory. *Internat J Numer Methods Engrg* 2009;78(1):32–47. <http://dx.doi.org/10.1002/nme.2472>.
- [13] Huang Q, Cruse TA. Some notes on singular integral techniques in boundary element analysis. *Internat J Numer Methods Engrg* 1993;36(15):2643–59. <http://dx.doi.org/10.1002/nme.1620361509>, <https://onlinelibrary.wiley.com/doi/10.1002/nme.1620361509>.
- [14] Guiggiani M, Gigante A. A general algorithm for multidimensional cauchy principal value integrals in the boundary element method. *J Appl Mech Trans ASME* 1990;57(4):906–15. <http://dx.doi.org/10.1115/1.2897660>.
- [15] Qin X, Fan Y, Li H, Lei W. A direct method for solving singular integrals in three-dimensional time-domain boundary element method for elastodynamics. *Mathematics* 2022;10(2). <http://dx.doi.org/10.3390/math10020286>.
- [16] Gray LJ, Glaeser JM, Kaplan T. Direct evaluation of hypersingular Galerkin surface integrals. *SIAM J Sci Comput* 2004;25(5):1534–56. <http://dx.doi.org/10.1137/S1064827502405999>.
- [17] Klöckner A, Barnett A, Greengard L, O’Neil M. Quadrature by expansion: A new method for the evaluation of layer potentials. *J Comput Phys* 2013;252:332–49. <http://dx.doi.org/10.1016/j.jcp.2013.06.027>, [arXiv:1207.4461](https://arxiv.org/abs/1207.4461).
- [18] Scuderi L. A new smoothing strategy for computing nearly singular integrals in 3D Galerkin BEM. *J Comput Appl Math* 2009;225(2):406–27. <http://dx.doi.org/10.1016/j.cam.2008.07.052>.
- [19] Qin X, Zhang J, Xie G, Zhou F, Li G. A general algorithm for the numerical evaluation of nearly singular integrals on 3D boundary element. *J Comput Appl Math* 2011;235(14):4174–86. <http://dx.doi.org/10.1016/j.cam.2011.03.012>.
- [20] Gao XW, Yang K, Wang J. An adaptive element subdivision technique for evaluation of various 2D singular boundary integrals. *Eng Anal Bound Elem* 2008;32(8):692–6. <http://dx.doi.org/10.1016/j.enganabound.2007.12.004>.
- [21] Zhang J, Wang P, Lu C, Dong Y. A spherical element subdivision method for the numerical evaluation of nearly singular integrals in 3D BEM. *Eng Comput (Swansea, Wales)* 2017;34(6):2074–87.
- [22] Niu Z, Cheng C, Zhou H, Hu Z. Analytic formulations for calculating nearly singular integrals in two-dimensional BEM. *Eng Anal Bound Elem* 2007;31(12):949–64. <http://dx.doi.org/10.1016/j.enganabound.2007.05.001>.
- [23] Nintcheu Fata S. Semi-analytic treatment of nearly-singular Galerkin surface integrals. *Appl Numer Math* 2010;60(10):974–93. <http://dx.doi.org/10.1016/j.apnum.2010.06.003>, <https://linkinghub.elsevier.com/retrieve/pii/S0168927410001157>.
- [24] Sorgentone C, Tornberg A-K. A highly accurate boundary integral equation method for surfactant-laden drops in 3D. *J Comput Phys* 2018;360:167–91. <http://dx.doi.org/10.1016/j.jcp.2018.01.033>, <https://linkinghub.elsevier.com/retrieve/pii/S0021999118300433>.
- [25] Johnston BM, Johnston PR, Elliott D. A new method for the numerical evaluation of nearly singular integrals on triangular elements in the 3D boundary element method. *J Comput Appl Math* 2013;245(1):148–61. <http://dx.doi.org/10.1016/j.cam.2012.12.018>.
- [26] Han Z, Pan W, Cheng C, Hu Z, Niu Z. A semi-analytical treatment for nearly singular integrals arising in the isogeometric boundary element method-based solutions of 3D potential problems. *Comput Methods Appl Mech Engrg* 2022;398:115179. <http://dx.doi.org/10.1016/j.cma.2022.115179>, <https://linkinghub.elsevier.com/retrieve/pii/S0045782522003401>.
- [27] Izzo F, Runborg O, Tsai R. Corrected trapezoidal rules for singular implicit boundary integrals. *J Comput Phys* 2022;461:111193. <http://dx.doi.org/10.1016/j.jcp.2022.111193>.
- [28] Aimi A, Di Credico G, Diligenti M, Guardasoni C. Highly accurate quadrature schemes for singular integrals in energetic BEM applied to elastodynamics. *J Comput Appl Math* 2022;410:114186. <http://dx.doi.org/10.1016/j.cam.2022.114186>.
- [29] Tausch J. Adaptive quadrature rules for Galerkin BEM. *Comput Math Appl* 2022;113(2021):270–81. <http://dx.doi.org/10.1016/j.camwa.2022.03.030>.
- [30] Pözl D, Schanz M. Space-time discretized retarded potential boundary integral operators: Quadrature for collocation methods. *SIAM J Sci Comput* 2019;41(6):A3860–86. <http://dx.doi.org/10.1137/19M1245633>, <https://epubs.siam.org/doi/10.1137/19M1245633>.
- [31] Tlupova S, Beale JT. Regularized single and double layer integrals in 3D Stokes flow. *J Comput Phys* 2019;386:568–84. <http://dx.doi.org/10.1016/j.jcp.2019.02.031>, [arXiv:1808.02177](https://arxiv.org/abs/1808.02177).
- [32] Lei W, Li H, Qin X, Chen R, Ji D. Dynamics-based analytical solutions to singular integrals for elastodynamics by time domain boundary element method. *Appl Math Model* 2018;56:612–25. <http://dx.doi.org/10.1016/j.apm.2017.12.019>.
- [33] Ren Q, Chan CL. Analytical evaluation of the BEM singular integrals for 3D Laplace and Stokes flow equations using coordinate transformation. *Eng Anal Bound Elem* 2015;53:1–8. <http://dx.doi.org/10.1016/j.enganabound.2014.11.018>.
- [34] Ravnik J. An implementation of analytic expressions for singular integration in BEM. 2022, available at <https://github.com/transport-phenomena/BEM-singular-integrals>, (Accessed: 15.6.2022).
- [35] Šušnjara A, Verhnjak O, Poljak D, Cvetković M, Ravnik J. Stochastic-deterministic boundary element modelling of transcranial electric stimulation using a three layer head model. *Eng Anal Bound Elem* 2021;123:70–83. <http://dx.doi.org/10.1016/j.enganabound.2020.11.010>, <https://linkinghub.elsevier.com/retrieve/pii/S0955799720302939>.
- [36] Šušnjara A, Verhnjak O, Poljak D, Cvetković M, Ravnik J. Uncertainty quantification and sensitivity analysis of transcranial electric stimulation for 9-subdomain human head model. *Eng Anal Bound Elem* 2022;135:1–11. <http://dx.doi.org/10.1016/j.enganabound.2021.10.026>.
- [37] Štrahl M, Wedel J, Steinmann P, Hriberšek M, Ravnik J. Numerical drag and lift prediction framework for superellipsoidal particles in multiphase flows. *Int J Comput Methods Exp Meas* 2022;10(1):38–49. <http://dx.doi.org/10.2495/CMEM-V10-N1-38-49>.
- [38] Štrahl M, Hriberšek M, Wedel J, Steinmann P, Ravnik J. A Model for Translation and Rotation Resistance Tensors for Superellipsoidal Particles in Stokes Flow. *J Mar Sci Eng* 2022;10:369. <http://dx.doi.org/10.3390/jmse10030369>.
- [39] Wrobel LC. *The boundary element method*. John Wiley & Sons, LTD; 2002.
- [40] Pozrikidis C. *Introduction to theoretical and computational fluid dynamics*. USA: Oxford University Press; 2011.
- [41] Weißer S. Residual based error estimate and quasi-interpolation on polygonal meshes for high order BEM-based FEM. *Comput Math Appl* 2017;73(2):187–202. <http://dx.doi.org/10.1016/j.camwa.2016.11.013>, <https://linkinghub.elsevier.com/retrieve/pii/S0898122116306307>.
- [42] Stokes GG. On the theories of internal friction of fluids in motion and of the equilibrium and motion of elastic solids. *Trans Camb Phil Soc* 1845;8:287–319.